Electrocatalysis

Deutsche Ausgabe: DOI: 10.1002/ange.201501419
Internationale Ausgabe: DOI: 10.1002/anie.201501419

Phosphorus-Modified Tungsten Nitride/Reduced Graphene Oxide as a High-Performance, Non-Noble-Metal Electrocatalyst for the Hydrogen Evolution Reaction**

Haijing Yan, Chungui Tian, Lei Wang, Aiping Wu, Meichen Meng, Lu Zhao, and Honggang Fu**

Abstract: *Phosphorus-modified tungsten nitride/reduced graphene oxide (P-WN/rGO) is designed as a high-efficient, low-cost electrocatalyst for the hydrogen evolution reaction (HER). WN (ca. 3 nm in size) on rGO is first synthesized by using the $H_3[PO_4(W_3O_9)_4]$ cluster as a W source. Followed by phosphorization, the particle size increase slightly to about 4 nm with a P content of 2.52 at%. The interaction of P with rGO and WN results in an obvious increase of work function, being close to Pt metal. The P-WN/rGO exhibits low onset overpotential of 46 mV, Tafel slope of 54 mV dec^{-1}, and a large exchange current density of 0.35 mA cm^{-2} in acid media. It requires overpotential of only 85 mV at current density of 10 mA cm^{-2}, while remaining good stability in accelerated durability testing. This work shows that the modification with a second anion is powerful way to design new catalysts for HER.*

Hydrogen, as a clean renewable energy source of fuel, is one of the most promising energy carriers for replacing traditional fossil fuels.[1] Electrolysis of water is considered the simplest way to produce hydrogen of high purity at the most economical price.[2] An efficient hydrogen evolution reaction (HER) catalyst is usually required to reduce the overpotential (η) in the HER process. The ideal catalysts for the HER should achieve the large exchange current and the small Tafel slope. Pt is the most popular catalyst, with high exchange current density (j_0), small Tafel slope and robust stability.[3] However, the use of Pt is limited owing to its scarcity and high cost, which push forward the intensive study on the cost-effective alternative to Pt catalyst.

Low-cost and active HER catalysts have been explored, such as cheap metal Ni, Ni-based alloy, sulfide, selenide, and non-metal composites.[4] MoS_2, as the earliest and representative non-Pt catalyst for the HER, can usually give an η in the range of 100–200 mV. By the rational tuning of cations and anions, active catalysts can be designed, such as CoS_2, FeS, NiS, $CoSe_2$, $MoSe_2$, and MoN.[5] Transition-metal phosphides (TMPs) are an important class of catalyst owing to their wide range of compositions, crystal structures, and accessible electronic states.[6] Most recently, the phosphides (Ni_2P, CoP, FeP) as active and robust HER catalysts were demonstrated, which open a new area in designing HER catalysts.[7] The promising activity of phosphides is considered to be related with the function of P; that is, it possess lone-pair electrons in 3p orbitals and vacant 3d orbitals, and can induce local charge density and accommodate the surface charge state.[8]

The tungsten-based compounds are an important family of catalysts. The combination of W with S, C, N, and P can form active catalysts useful for methanol oxidation, the ORR, and DSSCs.[9] WN (W_2N) are known as original hydrodesulfurization (HDS) catalysts owing to their Pt-like characteristics.[10] The reversible binding and dissociation of H_2 represents a possible mechanistic commonality of HDS and HER, implying that the WN should be potential catalyst for HER. The similar electronic structure of W with Mo has also supported the speculation. Theoretical calculations predict that the hydrogen is inclined to adsorb on the metal nitride surface, making the reaction easily happen. Recently, amorphous W_2N nanoparticles (NPs) have been developed as a catalyst for the HER in acidic solutions, but with relative low activity.[11] Therefore, ways to enhance the catalytic activity of tungsten-nitride based HER catalysts remains a challenge. We wondered whether a rational modification of P on WN can be used to enhance the activity of tungsten nitride catalysts based on the vital function of phosphorus in the HER and the influence of P on the electronic state of metal elements, thus giving a significant effect on catalytic properties.[8] Small-size WN (ca. 3 nm) on rGO is selected as a model to test this idea. We found that the P modification can lead significant enhancements in catalytic activity and stability for the HER in acidic media. The P-modified WN/rGO (P-WN/rGO) exhibits a very small onset overpotential of 46 mV, low Tafel slope of 54 mV dec^{-1}, and large exchange current density of 0.35 mA cm^{-2}. Furthermore, it requires an overpotential of only 85 mV at a current density of 10 mA cm^{-2}. Recently, Jaramillo and Kibsgaard have shown that the replacement of P in MoP with S anions can produce more active catalyst, namely MoP | S.[12] Our work shows that the rational modification with secondary anions is powerful way to design active and stable catalysts for HER, further verifying the importance of anions for HER.

[*] Dr. H. Yan, Prof. C. Tian, Dr. L. Wang, Dr. A. Wu, M. Meng, L. Zhao, Prof. H. Fu
Key Laboratory of Functional Inorganic Material Chemistry
Ministry of Education of the People's Republic of China
Heilongjiang University, Harbin 150080 (China)
E-mail: chunguitianhq@163.com
fuhg@vip.sina.com

[**] This work was supported by the NSFC of China (21031001, 91122018, 21371053, 21101061) and the Program for Innovative Research Team in University (IRT-1237).

Supporting information for this article is available on the WWW under http://dx.doi.org/10.1002/anie.201501419.

The P-WN/rGO was prepared by phosphorization of small-sized WN (ca. 3 nm) on rGO (WN/rGO) by using NaH_2PO_2 as P source (see the Supporting Information). The use of the small-sized WN/rGO to obtain small-sized P-WN/rGO is based on the consideration that the small size will provide a highly accessible surface, thus promoting the catalytic activity of the materials. X-ray diffraction (XRD) patterns (Supporting Information, Figure S1) show the characteristic peaks of graphite[13] for P-rGO, and reflections of crystalline hexagonal WN[10] for WN/rGO. The great suppression of the strong (002) peak of rGO can be attributed to the loading of WN with high density and good crystallinity. The P-WN/rGO shows similar peaks with WN/rGO while there is no obvious diffraction of WP. However, in comparison with WN/rGO, the peaks have a small shift towards smaller angles, implying the introduction of the larger anions (P) than N.

The state of P in P-WN/rGO are analyzed by X-ray photoelectron spectroscopy (XPS). The wide-scan spectrum (Supporting Information, Figure S2) shows the presence of P in P-WN/GO, along with the elements O, C, N, and W. The high-resolution XPS spectrum (HRXPS) of P (Figure 1 a) can

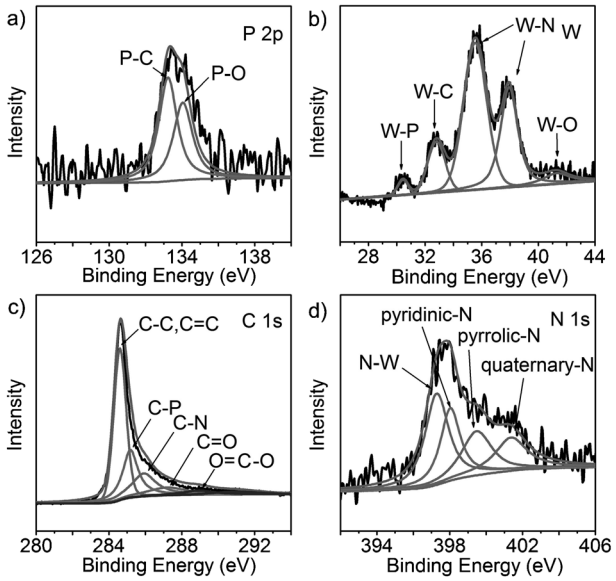

Figure 1. XPS spectra of a) P, b) W, c) C, and d) N in P-WN/rGO.

be mainly deconvoluted into two sub-peaks located at 133.3 and 134.4 eV, ascribed to the P–C and P–O bond, respectively.[14] The peak related with P combined with W[15] (about 130.1 eV) is not obvious. However, after overlaid three sets of parallel XPS data of P 2p, a peak at 130.1 eV assigned to the P–W can be observed (Supporting Information, Figure S3). The HRXPS of W also shows the obvious peak about W combined with P (Figure 1 b), implying the presence of interaction of W with P. For P-rGO, the binding energy of P–C ($BE_{P\text{-}C}$) and P–O ($BE_{P\text{-}O}$) can be seen at 132.5 eV and 133.8 eV, respectively (Supporting Information, Figure S4a). The positive shift of 0.8 eV for BE_{P-C} and 0.6 eV for BE_{P-O} are obvious by comparing P-WN/rGO with P-rGO. The result indicates that the electrons in P can be transferred into WN in P-WN/rGO.[16] The increase of electrons on WN can facilitate the absorption of H^+ for subsequent HER. Furthermore, the intensity ratio of P–C and P–O peaks for P-WN/rGO is larger than 1, but it is much less than 1 for P-rGO. The content of P–C in P-WN/rGO and P-rGO is about 1.4 at % and 0.5 at % based on quantitative results from XPS. The result suggests that more phosphorus atoms are incorporated into the carbon framework in P-WN/rGO, which should be favorable for enhancing the activity in electrocatalysis.[14] The percentage of P is about 2.52 at % for P-WN/rGO, which is much higher than 1.25 at % for P-rGO. The P can also be detected in WN/rGO (0.53 at %). The P should be from the $H_3[PO_4(W_3O_9)_4]$ (PW_{12}), which is a reason of choosing PW_{12} as precursor (Supporting Information, Figure S4b). The amount of P in P-WN/rGO is higher than sum of that in WN/rGO and P-rGO, implying that the presence of WN is favorable for fixing of P. The HRXPS of C and O indicates the presence of P–C (Figure 1 c) and P-O (Supporting Information, Figure S4c), further supporting the results from P spectra. The presence of N with dominant N–W bond can be observed (Figure 1 d), indicating that WN is the main phase of the W component.

The combination of the above investigations indicates that the P-WN/rGO is formed by the nitridation and subsequent phosphorization of PW_{12}. In the process, the GO support also underwent some change. As is known, the relative intensity ratio of D and G bands is a measure of disorder degree of carbon materials.[17] As shown in the Supporting Information, Figure S5, the intensity ratio of D/G peak (I_D/I_G) of P-WN/rGO (0.98) is larger than those of P-rGO (0.80) and WN/rGO (0.94). The higher value of I_D/I_G of P-WN/rGO than of WN/rGO is contributed to the formation C–P bond that induced additional structural disorder.[18] The increase of I_D/I_G of P-WN/rGO in comparison to that of P-rGO contributes to the strong interaction of NPs with support. The result also implies the introduction of P into WN/rGO and presence of the interaction between P with WN and rGO, which should be favorable to improve the activity of P-WN/rGO.

The scanning electron microscopy (SEM) image and transmission electron microscopy (TEM) images of P-WN/rGO reveal the formation of the small-sized and high-dispersed particles on rGO with high density (Figure 2). A high-resolution TEM (HRTEM) image and FFT show the lattice fringes with a *d* spacing of 0.25 nm, corresponding to the (100) plane of WN (Figure 2 c). The particles are mainly in 4 nm in size (Figure 2 c,d). The size is slightly larger than that about 3 nm in WN/rGO (Supporting Information, Figure S6a), which should be due to the aggregation and growth under the phosphorization process. When the same procedure is performed without use of rGO, particles with a size of about 50 nm are obtained (Supporting Information, Figure S6b), indicating the importance of rGO to restrict the growth of WN. The role of rGO should be relative with their special plane structure and plentiful groups, which are suitable for the growth of NPs[19,20] and the role of modified PEI on anchoring PW_{12} clusters.[9a]

For the HER process, the electrons on the catalyst will react with H^+ to form H atoms. A good catalyst should trap more electrons to facilitate the occurrence of the reaction.

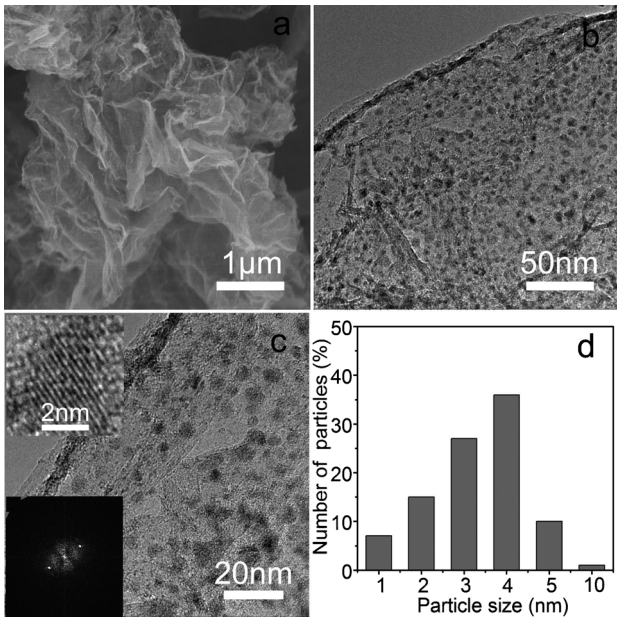

Figure 2. a) SEM image of P-WN/rGO. b), c) TEM images of P-WN/rGO. The insets in (c) are a HRTEM image (upper) and a FFT spectrum of the WN. d) Size distribution of NPs in P-WN/rGO.

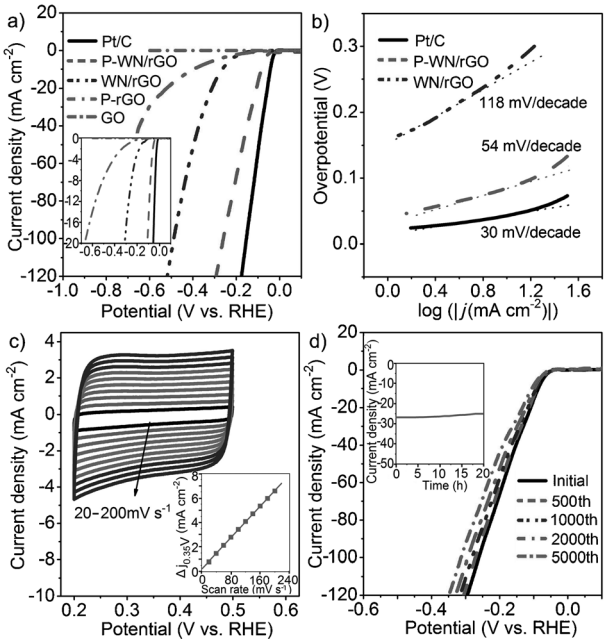

Figure 3. a) Polarization curves for P-WN/rGO, WN/rGO, P-rGO, Pt/C, and GO in 0.5 M H_2SO_4 with a scan rate of 5 mV s^{-1}. b) Tafel plots for P-WN/rGO, WN/rGO and Pt/C. (c) CVs for P-WN/rGO with different rates from 20 to 200 mV s^{-1}. The inset in (c) is the capacitive current at 0.35 V as a function of scan rate for P-WN/rGO ($\Delta j_0 = j_a - j_c$). d) Polarization data for the P-WN/rGO sample in 0.5 M H_2SO_4 initially and after 500, 1000, 2000, and 5000 CV sweeps between +0.1 and −0.3 V vs RHE. The inset in (d) is the time dependence of the current density for P-WN/rGO at a static overpotential of 120 mV for 20 h.

The surface work function represents the ability of catalyst to trap electrons. The Pt metal have excellent catalytic properties for the HER owing to its high work function, which is favorable to trap electrons.[21] The work function is effected by the surface modification with atom and molecules. The role of P modification is confirmed by a scanning Kelvin probe test (SKP). The SKP is an extremely sensitive instrument capable of discerning subtle molecular interactions using vibrating electromagnetic and acoustic fields. SKP images of materials can give signals that indicate a distinct potential change, which signifies a remarkable work-function change (Supporting Information, Figure S7). The work function values of P-WN/rGO, WN/rGO, P-rGO, and Pt black are about 5.58, 5.43, 5.38, and 5.60 eV, respectively. The higher work function of P-WN/rGO than WN/rGO implies the enhanced ability to trap the electrons after P modification. Notably, the work function of P-WN/rGO is close to that of Pt, implying the large potential of P-WN/rGO as promising like-Pt catalyst for HER.

The catalytic performance for the HER were tested by depositing the catalysts with the same loading of approximately 0.337 mg cm^{-2} on a glassy carbon electrode (GCE; see the Supporting Information). Five catalysts, including P-WN/rGO, WN/rGO, P-rGO, GO, and commercial Pt/C (20 wt %), were examined. Figure 3a shows the polarization curves without IR compensation. The Pt/C catalyst shows excellent HER activity. Although GO gives poor performance, the P-rGO have improved activity with an onset overpotential (vs RHE) of 197 mV, indicating the positive role of P modification for the HER. It is seen that WN/rGO reveals a large cathodic current density with a small onset overpotential of 114 mV. As expected, the P-WN/rGO exhibits an onset overpotential of 46 mV, which is more superior to the corresponding WN/rGO. The current densities are 2 and 10 mA cm^{-2} at overpotential of 56 and 85 mV, respectively, for P-WN/rGO, whereas WN/rGO needs an overpotential of 265 mV to reach a current density of 10 mA cm^{-2}. It was determined by XPS that the P accounts about 37 % of the total amount of P and N atoms in P-WN/rGO (Supporting Information, Table S1). Despite the lower amount of P, its modification can dramatically enhance the catalytic performance of WN/rGO. The value for P-WN/rGO is better than those of Mo (W)-based and some phosphide catalysts in acidic media, such as MoS_2/RGO, WS_2, Mo_2C, NiMoNx/C, $Co_{0.6}Mo_{1.4}N_2$, W_2C, Cu_3P, MoP, and Ni_2P[22,7a] (Supporting Information, Table S2). Furthermore, P-WN/rGO gives an exchange current density of 0.35 mA cm^{-2} (Supporting Information, Figure S8). It is higher than that of WN/rGO (0.16 mA cm^{-2}) and most values for non-noble-metal HER catalysts (Supporting Information, Table S2). The Tafel plots are fit to the Tafel equation $\eta = b\log(j) + a$, where j is the current density and b is the Tafel slope, yielding Tafel slopes of approximately 30, 54, and 118 mV dec^{-1} for Pt/C, P-WN/rGO, and WN/rGO (Figure 3b), respectively. The Tafel slopes for both P-WN/rGO and WN/rGO catalysts do not match the expected Tafel slopes of 29, 38, and 116 mV dec^{-1} correlating with a different rate-determining step of HER, revealing that the HER proceeds through a Volmer–Heyrovsky mechanism.[7a,c]

The electrochemical surface area is used as an approximate guide for surface roughness within an order-of-magnitude accuracy.[23] To estimate the effective surface areas, we

measured the capacitance of the double layer at the solid–liquid interface. The cyclic voltammograms (CVs) were collected in the region of 0.2–0.5 V, where the current response should be only due to the charging of the double layer (Figure 3c). The capacitance of P-WN/rGO is 32 mF cm^{-2}, which is much higher than WN/rGO (11 mF cm^{-2}; Supporting Information, Figure S9). Thus, the large exchange current density of P-WN/rGO can be associated with its high surface area.

Accelerated degradation test is performed to evaluate the stability. CV sweeps between +0.1 and −0.3 V are applied. After 5000 CV sweeps, the LSV curve exhibits 34 mV loss at current density of 10 mA cm^{-2} (Figure 3d). In contrast, for WN/rGO, a significant loss of 111 mV had occurred after the 5000 cycles (Supporting Information, Figure S10). The inset in Figure 3d shows the time dependence of the current density for P-WN/rGO at an overpotential of 120 mV, suggesting that the catalyst maintains 92% of the initial current density for 20 h of test. For WN/rGO, however, only approximately 80% of the current density were maintained in the same period (Supporting Information, Figure S10, inset). These results suggest that P-WN/rGO has superior stability in a long-term electrochemical process.

The superior HER activity of P-WN/rGO can be attributed to the following reasons. As indicated by work function, differential charge distinct interfacial polarization occurs after the modification of P atoms into the WN/rGO, resulting in substantial negative charges on the surface of catalyst. For the HER ($2H^+ + 2e^- \rightleftharpoons H_2$), the increase of electron density on the catalyst surface surely improves the reaction activity. Thus, H^+ are more easily adsorbed on the surface of P-WN/rGO with abundant negative charges to produce H_2. The small size of the WN NPs in the hybrid favors also the exposure of more active sites for H^+ adsorption, as well as the excellent electrical conductivity of rGO support facilitates charge transfer in the hybrid.

In summary, we have demonstrated that P-modified WN/rGO can be used as active, low-cost, non-noble metal electrocatalyst for theHER. The catalyst exhibits a superior activity with a low onset overpotential of 46 mV, Tafel slope of 54 mV dec^{-1}, a large exchange current density of 0.35 mA cm^{-2}, and good stability. The enhanced performance of P-WN/rGO should be relative with the interaction of P with rGO and WN. Also, we think that the performance of P-WN/rGO can be further improved by loading the catalyst on Ti plate[12] with high loading, or by growth of the catalyst on carbon cloth to form a 3D catalyst.[22g] Further work is under way. Our work shows that the modification with second anions is powerful way to design robust catalysts for the HER.

Keywords: electrocatalysis · hydrogen evolution reaction · phosphorus · reduced graphene oxide · tungsten nitrides

How to cite: *Angew. Chem. Int. Ed.* **2015**, *54*, 6325–6329
Angew. Chem. **2015**, *127*, 6423–6427

[1] a) M. S. Dresselhaus, I. L. Thomas, *Nature* **2001**, *414*, 332–337; b) J. A. Turner, *Science* **2004**, *305*, 972–974.
[2] H. M. Chen, C. K. Chen, R. S. Liu, L. Zhang, J. J. Zhang, D. P. Wilkinson, *Chem. Soc. Rev.* **2012**, *41*, 5654–5671.
[3] a) M. G. Walter, E. L. Warren, J. R. McKone, S. W. Boettcher, Q. X. Mi, E. A. Santori, N. S. Lewis, *Chem. Rev.* **2010**, *110*, 6446–6473; b) S. Bai, C. M. Wang, M. S. Deng, M. Gong, Y. Bai, J. Jiang, Y. J. Xiong, *Angew. Chem. Int. Ed.* **2014**, *53*, 12120–12124; *Angew. Chem.* **2014**, *126*, 12316–12320.
[4] a) J. R. McKone, B. F. Sadtler, C. A. Werlang, N. S. Lewis, H. B. Gray, *ACS Catal.* **2013**, *3*, 166–169; b) Y. Choquette, L. Brossard, A. Lasia, H. Ménard, *Electrochim. Acta* **1990**, *35*, 1251–1256; c) T. F. Jaramillo, K. P. Jørgensen, J. Bonde, J. H. Nielsen, S. Horch, I. Chorkendorff, *Science* **2007**, *317*, 100–102; d) D. S. Kong, H. T. Wang, J. J. Cha, M. Pasta, K. J. Koski, J. Yao, Y. Cui, *Nano Lett.* **2013**, *13*, 1341–1347; e) J. J. Duan, S. Chen, M. Jaroniec, S. Z. Qiao, *ACS Nano* **2015**, *9*, 931–940; f) Y. Zheng, Y. Jiao, M. Jaroniec, S. Z. Qiao, *Angew. Chem. Int. Ed.* **2015**, *54*, 52–65; *Angew. Chem.* **2015**, *127*, 52–66.
[5] a) Y. Y. Duan, Q. W. Tang, J. Liu, B. L. He, L. M. Yu, *Angew. Chem. Int. Ed.* **2014**, *53*, 14569–14574; *Angew. Chem.* **2014**, *126*, 14797–14802; b) S. J. Peng, L. L. Li, X. P. Han, W. P. Sun, M. Srinivasan, S. G. Mhaisalkar, F. Y. Cheng, Q. Y. Yan, J. Chen, S. Ramakrishna, *Angew. Chem. Int. Ed.* **2014**, *53*, 12594–12599; *Angew. Chem.* **2014**, *126*, 12802–12807; c) Z. H. Dai, S. H. Liu, J. C. Bao, H. X. Ju, *Chem. Eur. J.* **2009**, *15*, 4321–4326; d) H. C. Sun, D. Qin, S. Q. Huang, X. Z. Guo, D. M. Li, Y. H. Luo, Q. B. Meng, *Energy Environ. Sci.* **2011**, *4*, 26300–26307; e) M. X. Wu, Q. Y. Zhang, J. Q. Xiao, C. Y. Ma, X. Lin, C. Y. Miao, Y. J. He, Y. R. Gao, A. Hagfeldt, T. L. Ma, *J. Mater. Chem.* **2011**, *21*, 10761–10766.
[6] S. Carenco, D. Portehault, C. Boissière, N. Mézailles, C. Sanchez, *Chem. Rev.* **2013**, *113*, 7981–8065.
[7] a) E. J. Popczun, J. R. McKone, C. G. Read, A. J. Biacchi, A. M. Wiltrout, N. S. Lewis, R. E. Schaak, *J. Am. Chem. Soc.* **2013**, *135*, 9267–9270; b) E. J. Popczun, C. G. Read, C. W. Roske, N. S. Lewis, R. E. Schaak, *Angew. Chem. Int. Ed.* **2014**, *53*, 5427–5430; *Angew. Chem.* **2014**, *126*, 5531–5534; c) P. Jiang, Q. Liu, Y. H. Liang, J. Q. Tian, A. M. Asiri, X. P. Sun, *Angew. Chem. Int. Ed.* **2014**, *53*, 12855–12859; *Angew. Chem.* **2014**, *126*, 13069–13073.
[8] D. S. Yang, D. Bhattacharjya, S. Inamdar, J. Park, J. S. Yu, *J. Am. Chem. Soc.* **2012**, *134*, 16127–16130.
[9] a) H. J. Yan, C. G. Tian, L. Sun, B. Wang, L. Wang, J. Yin, A. P. Wu, H. G. Fu, *Energy Environ. Sci.* **2014**, *7*, 1939–1949; b) Y. Liu, W. E. Mustain, *ACS Catal.* **2011**, *1*, 212–220; c) D. Braga, I. G. Lezama, H. Berger, A. F. Morpurgo, *Nano Lett.* **2012**, *12*, 5218–5223; d) J. S. Jang, D. J. Ham, E. Ramasamy, J. Lee, J. S. Lee, *Chem. Commun.* **2010**, *46*, 8600–8602.
[10] J. G. Chen, *Chem. Rev.* **1996**, *96*, 1477–1498.
[11] W. F. Chen, J. T. Muckerman, E. Fujita, *Chem. Commun.* **2013**, *49*, 8896–8909.
[12] J. Kibsgaard, T. F. Jaramillo, *Angew. Chem. Int. Ed.* **2014**, *53*, 14433–14437; *Angew. Chem.* **2014**, *126*, 14661–14665.
[13] R. H. Wang, Y. Xie, K. Y. Shi, J. Q. Wang, C. G. Tian, P. K. Shen, H. G. Fu, *Chem. Eur. J.* **2012**, *18*, 7443–7451.
[14] W. Zhang, Z. Y. Wu, H. L. Jiang, S. H. Yu, *J. Am. Chem. Soc.* **2014**, *136*, 14385–14388.
[15] Z. C. Xing, Q. Liu, A. M. Asiri, X. P. Sun, *ACS Catal.* **2015**, *5*, 145–149.
[16] J. Yang, Y. Xie, R. H. Wang, B. J. Jiang, C. G. Tian, G. Mu, J. Yin, B. Wang, H. G. Fu, *ACS Appl. Mater. Interfaces* **2013**, *5*, 6571–6579.
[17] S. Stankovich, D. A. Dikin, R. D. Piner, K. A. Kohlhaas, A. Kleinhammes, Y. Y. Jia, Y. Wu, S. T. Nguyen, R. S. Ruo, *Carbon* **2007**, *45*, 1558–1565.
[18] S. Reich, C. Thomsen, *Philos. Trans. R. Soc. A* **2004**, *362*, 2271–2288.

[19] X. M. Chen, G. H. Wu, J. M. Chen, X. Chen, Z. X. Xie, X. R. Wang, *J. Am. Chem. Soc.* **2011**, *133*, 3693 – 3695.
[20] Q. Zhang, C. G. Tian, A. P. Wu, T. X. Tan, L. Sun, L. Wang, H. F. Fu, *J. Mater. Chem.* **2012**, *22*, 11778 – 11784.
[21] H. B. Michaelson, *J. Appl. Phys.* **1977**, *48*, 4729 – 4733.
[22] a) Y. G. Li, H. L. Wang, L. M. Xie, Y. Y. Liang, G. S. Hong, H. J. Dai, *J. Am. Chem. Soc.* **2011**, *133*, 7296 – 7299; b) D. Voiry, H. Yamaguchi, J. W. Li, R. Silva, D. C. B. Alves, T. Fujita, M. W. Chen, T. Asefa, V. B. Shenoy, G. Eda, M. Chhowalla, *Nat. Mater.* **2013**, *12*, 850 – 855; c) W. F. Chen, C. H. Wang, K. Sasaki, N. Marinkovic, W. Xu, J. T. Muckerman, Y. Zhu, R. R. Adzic, *Energy Environ. Sci.* **2013**, *6*, 943 – 951; d) W. F. Chen, K. Sasaki, C. Ma, A. I. Frenkel, N. Marinkovic, J. T. Muckerman, Y. M. Zhu, R. R. Adzic, *Angew. Chem. Int. Ed.* **2012**, *51*, 6131 – 6135; *Angew. Chem.* **2012**, *124*, 6235 – 6239; e) B. F. Cao, G. M. Veith, J. C. Neuefeind, R. R. Adzic, P. G. Khalifah, *J. Am. Chem. Soc.* **2013**, *135*, 19186 – 19192; f) A. T. Garcia-Esparza, D. Cha, Y. W. Ou, J. Kubota, K. Domen, K. Takanabe, *ChemSusChem* **2013**, *6*, 168 – 181; g) J. Q. Tian, Q. Liu, N. Y. Cheng, A. M. Asiri, X. P. Sun, *Angew. Chem. Int. Ed.* **2014**, *53*, 9577 – 9581; *Angew. Chem.* **2014**, *126*, 9731 – 9735; h) J. M. McEnaney, J. C. Crompton, J. F. Callejas, E. J. Popczun, A. J. Biacchi, N. S. Lewis, R. E. Schaak, *Chem. Mater.* **2014**, *26*, 4826 – 4831.
[23] S. Trasatt, O. A. Petri, *Pure Appl. Chem.* **1991**, *63*, 711 – 734.

Received: February 12, 2015
Published online: March 30, 2015

